25-29 August 2024
inter.noise
NANTES FRANCE

Reflectivity characterization of in-flow acoustic floor treatment for the NASA Langley 14- by 22-Foot Subsonic Tunnel

Nikolas S. Zawodny[1]
Kyle A. Pascioni[2]
Andrew H. Lind[3]
Matthew B. Galles[4]
Colin M. Stutz[5]
Mary L. Houston[6]
NASA Langley Research Center
Hampton, VA 23681

ABSTRACT

An experimental campaign was performed to assess acoustic modifications to the NASA Langley Research Center 14- by 22-Foot Subsonic Tunnel. Recent acoustic test campaigns in this facility have emphasized the reduction of aerodynamic noise due to flow scrubbing across acoustically treated floor baskets. However, the measures implemented to address this noise contaminant have resulted in the installation of floor basket coverings of high acoustic reflectivity. Therefore, a controlled test campaign was performed to identify a suitable acoustic basket configuration in terms of both acoustic absorptivity and reduced flow scrubbing noise. This test campaign was conducted in two phases: the first in an anechoic chamber facility on a single acoustic basket panel to identify a notional configuration of acceptable absorptivity, and the second in a complete floor basket installation checkout test in the NASA Langley 14- by 22-Foot Subsonic Tunnel. Results show that the newly implemented floor treatment exhibits suitable performance in both desired categories of acoustic absorptivity and reduced flow scrubbing noise. This campaign has also validated the effectiveness and usefulness of the anechoic chamber test configuration as a means of assessing acoustic reflections at oblique angles of incidence.

1. INTRODUCTION

The NASA Langley 14- by 22-Foot Subsonic Tunnel (14x22) has undergone a series of acoustic upgrades since the 1990s. Some of the first acoustic tests performed in this facility were on a model tiltrotor and focused on intense tonal acoustics due to rotor blade-vortex interactions (BVI) [1]. In recent years, focus has shifted towards measuring airframe noise of scaled vehicle models. The most recently tested of these configurations is the 10%-scale High-Lift Common Research Model (CRM-HL) [2]. Figure 1 provides images of the 14x22 test section for these test configurations.

[1]nikolas.s.zawodny@nasa.gov
[2]kyle.a.pascioni@nasa.gov
[3]andrew.h.lind@gmail.com
[4]matthew.b.galles@nasa.gov
[5]colin.m.stutz@nasa.gov
[6]mary.l.houston@nasa.gov

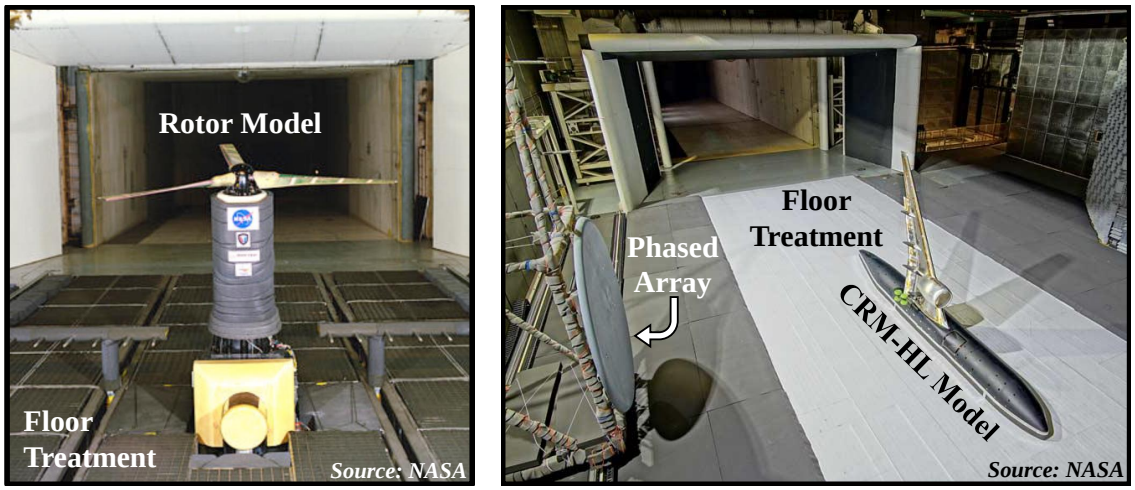

(a) Model Tiltrotor (1995) (b) CRM-HL (2021)

Figure 1: Images of the 14x22 test section configured for acoustic measurements of a (a) model tiltrotor and (b) scaled fixed-wing aircraft. *Note: Images represent views looking downstream.*

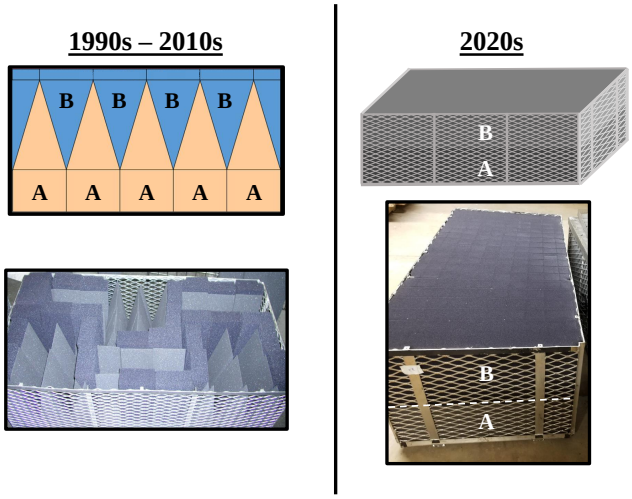

Figure 2: Photographs and notional representations of acoustic basket frame and fill materials. *[Source: NASA]*

Preparation for acoustic testing in the 14x22 is carried out by means of lowering the test section model cart floor (white region of Figure 1(b)) to allow for the installation of individual acoustic baskets. While several different basket sizes are required to fully occupy the test section floor, the majority of the baskets have common dimensions of 1.6 m long (streamwise) by 0.8 m wide (lateral) by 0.6 m deep. As Figure 2 shows, each acoustic basket is comprised of a porous metal frame into which open-cell acoustic foam is installed. Since the 1990s, the acoustic foam installation has changed from a series of inverted foam wedges of lower density (labeled B) stacked on top of upright foam wedges of similar height and of higher density (labeled A), to a simpler arrangement of stacked foam blocks of the same densities as the legacy wedges but with equal depths of 0.3 m. The reason for this change in acoustic treatment pattern was to simplify the installation process while not appreciably sacrificing the absorptive properties offered by the variable density of the foam layers.

As can be expected, there is a trade-off between the acoustic absorptivity and the aerodynamic scrubbing noise performances of acoustic treatments exposed to flow. As can be seen in Figure 3, the top surfaces of the baskets have changed over time. Circa 1995, the presence of bare-faced open-cell foam yielded favorable acoustic absorption behavior, however it also yielded prominent aerodynamic scrubbing noise. This was not an issue at the time, because the relative tonal noise levels of the rotor far surpassed the background noise. More recently, the CRM-HL test was designed to evaluate airframe noise generation at model-scale frequencies. Therefore, reduction of aerodynamic scrubbing noise was identified as the more immediate facility noise contaminant to address and mitigate. In doing so, the basket top design transitioned from a simple foam sheet held in place on top of the basket fill via a welded grid of steel rods (see Figure 3(a)), to a more intricate system of a similar grid with a series of interwoven foam strips and a sheet of perforate metal that was spot-welded to the grid (see Figure 3(b)). As is discussed in

more detail in Reference 3, covering this perforate sheet with an adhesive-backed felt was found to yield the lowest levels of aerodynamic scrubbing noise.

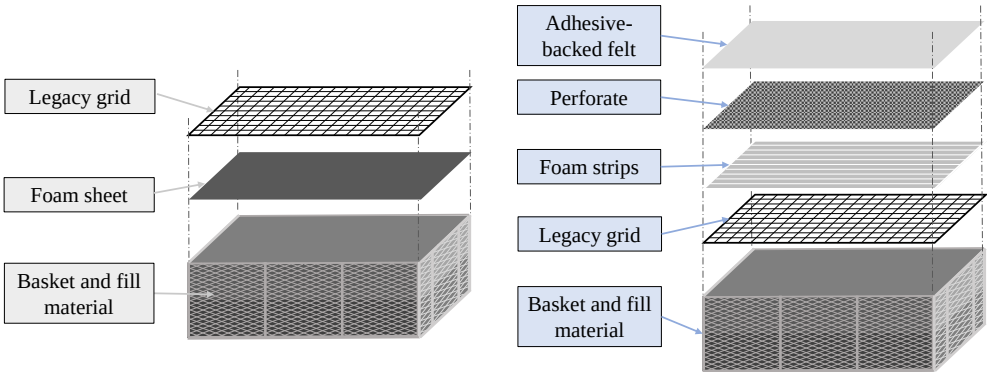

(a) 1990s-2010s (b) 2021

Figure 3: Illustrations of previous acoustic basket configurations.

The objectives of the current study are two-fold: (1) to identify the impacts of the latest acoustic basket top redesign on acoustic reflectivity, and (2) to identify and test the acoustic reflectivity and aerodynamic scrubbing performance of the newly proposed acoustic basket top treatment in a wind tunnel test configuration. The ultimate goal of this investigation is to build upon previous iterations and prove the effectiveness of a new acoustic basket top treatment. The new configuration should have a suitable acoustic absorptivity and low levels of aerodynamic scrubbing that will be generally applicable regardless of the frequency ranges of interest for a specific test.

2. TECHNICAL APPROACH

This experimental investigation is divided into two test campaigns: (1) controlled source tests on a single floor basket in an anechoic chamber to identify acoustic reflectivity, and (2) controlled source tests as well as empty facility operations in the 14x22 tunnel.

2.1. Anechoic Chamber Testing

The first phase of tests was conducted in the NASA Langley Structural Acoustics Loads and Transmission (SALT) anechoic chamber [4]. This facility is acoustically treated down to a cut-on frequency of 100 Hz and has interior dimensions (wedge tip to wedge tip) of 4.57-m (15-ft) high, 7.65-m (25-ft) wide, and 9.63-m (31.6-ft) long. A tower of three equally spaced free-field Brüel & Kjær 6.35 mm Type 4954 microphones were positioned across from a Mackie® HR824 speaker and a single acoustic basket was positioned according to the schematic and photograph shown in Figure 4. The primary goal of this setup was to ascertain the reflectivity of an acoustic basket outfit with a variety of basket top configurations at oblique angles of incidence. A total of seven different configurations were tested, which are summarized in Figure 5. Of these configurations, six involve an acoustic basket, while one is a reference condition consisting of the fully treated anechoic chamber without an acoustic basket installed (C1). The basket frame and fill material remained the same for all measurement runs. Ten different band-limited white noise (BLWN) waveforms were generated and output by the speaker for each test configuration. These waveforms represent nine individual octave bands with center frequencies from 63 Hz to 16 kHz, and a tenth waveform representing this entire span of frequencies.

2.2. Wind Tunnel Testing

The second phase of tests was conducted in the NASA Langley 14x22 wind tunnel. This phase of testing was comprised of a combination of controlled acoustic source tests in a static (no flow) test

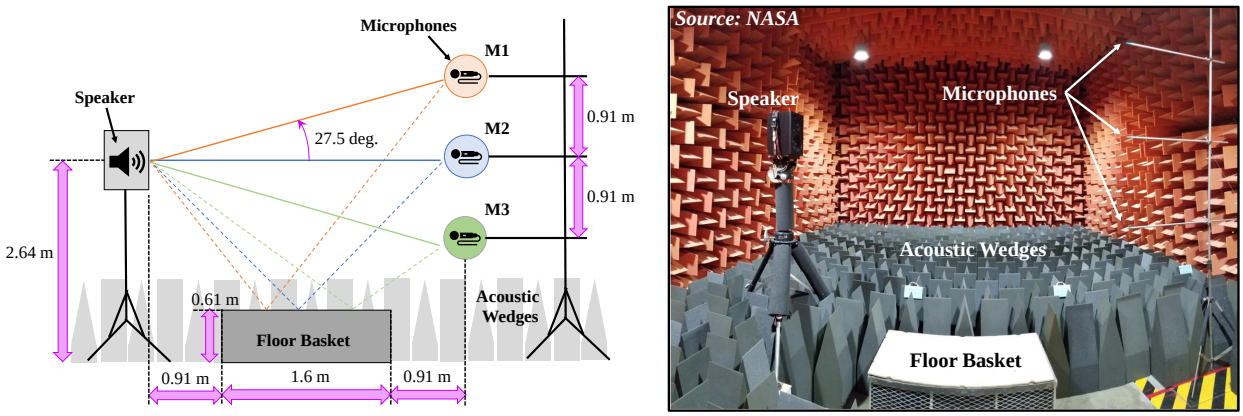

(a) Dimensioned Schematic

(b) Photograph of SALT chamber

Figure 4: SALT anechoic chamber test setup (a) dimensioned schematic and (b) photograph. *Note: photograph in (b) represents only partial test setup and is distorted due to panoramic mode of camera.*

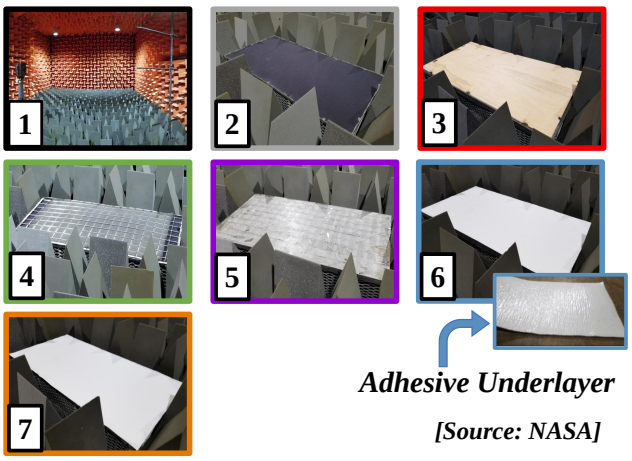

Config. #	Description
C1	Empty chamber (fully treated)
C2	Exposed fill material
C3	Plywood sheet
C4	Legacy grid*
C5	Perforate panel with legacy grid†
C6	Adhesive felt with perforate panel‡
C7	Non-adhesive felt over legacy grid

* See Figure 3(a)
† See Figure 3(b) without felt
‡ See Figure 3(b)

Figure 5: Photographs and descriptions of tested acoustic basket top configurations.

section, empty test section conditions at different flow speeds (background noise), and controlled acoustic source tests across a range of facility flow speeds. This paper focuses on the first two of these sets of test conditions, while the latter is addressed in two companion papers [5, 6]. The purpose of controlled acoustic source testing in a static environment is to assess the reflectivity of the new acoustic floor basket design in the absence of facility contamination effects due to flow-induced decorrelation and shear layer refraction. Static operations in such a facility have practical applications as well, such as for simulating hover conditions of rotor systems. Meanwhile, empty test section runs with flow are performed as a means of assessing the aerodynamic scrubbing noise due to flow over the new acoustic basket top surfaces relative to previous tests.

Figure 6 provides a schematic and photograph of the 14x22 open test section configured for acoustic testing. As can be seen in Figure 6(a), an acoustic source was placed at the lateral centerline of the test section, while a phased microphone array and linear tower microphone array were positioned outside of the flow on either side of the open test section. This study focuses on measurements made by the linear tower microphone array, while phased array measurements are discussed in Reference 6. The linear tower array is comprised of 11 free-field Brüel & Kjær 6.35-mm diameter Type 4939 microphones. The floor of the test section that is immersed in the freestream flow is comprised of a total of 80 acoustic baskets, while the out-of-flow floor sections are insulated with cloth-wrapped panels of fiberglass that measure 0.15 m in height and have a 0.1 m tall “ramp” of open cell foam as a flow barrier. Both microphone arrays have their own dedicated acoustic

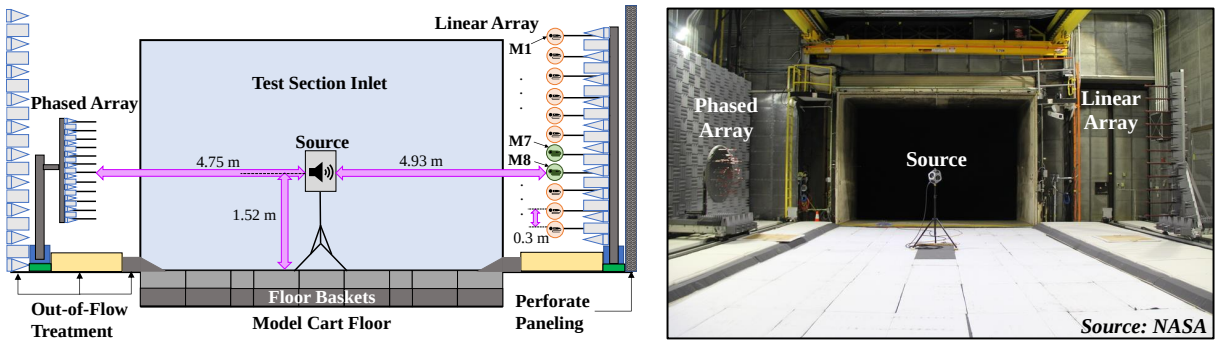

(a) Dimensioned Schematic (b) Photograph of 14x22 Test Section

Figure 6: Test setup in the 14x22 open test section. *Note: flow is out of the page for both images.*

treatment. While the facility north wall located behind the phased array (left side of Figure 6(a)) is treated with an array of 0.15 m tall foam wedges, the south wall behind the linear array (right side of Figure 6(a)) is outfitted with low-porosity perforate paneling that covers a variable depth of cloth-wrapped fiberglass insulation.

A total of four acoustic sources were tested in the 14x22. These sources were intended to diagnose different physical phenomena: overall facility reflections using an omnidirectional speaker at static conditions, direct-path reflections using a directional speaker at static conditions, lower-frequency signal-to-noise ratio assessments as a function of flow speed using a faired acoustic source, and higher-frequency signal-to-noise ratio assessments using this same fairing structure and a pneumatic airball source [7]. This phase of the study focuses on direct-path reflections under static conditions, which utilized the same Mackie® HR824 speaker as the SALT anechoic chamber test described in the Section 2.1. Information on the other acoustic sources used and tests implemented are documented in Reference 5.

To assess the relative absorptive behavior of the installed wind tunnel test section floor treatment, the top surfaces of a select set of acoustic baskets were modified in a manner similar to those presented in the previous section. Due to time constraints and installation complexity, only three basket top configurations were tested. These configurations are shown in Figure 7. Figure 7(a) shows a configuration intended to represent an in-situ reference condition (C1*), in

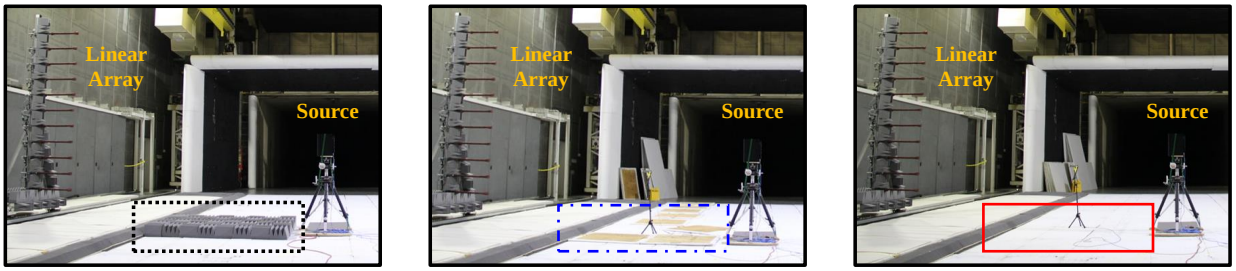

(a) Acoustic Wedges (C1*) (b) Plywood Panels (C3*) (c) Basket Tops (C7*)

Figure 7: Tested basket top configurations in the 14x22 test section. *Note: configuration labels can be related to their anechoic chamber counterparts in Figure 5. [Source: NASA]*

which the basket tops are lined with an array of 0.15 m tall acoustic wedges that span a length of 2.44 m towards the linear tower array, and 1.22 m wide. Figure 7(b) shows a configuration that represents an acoustically hard reference condition consisting of plywood panels (C3*) that span the same dimensions as the acoustic wedge coverings in Figure 7(a). Finally, Figure 7(c) shows a configuration that represents the newly designed basket tops intended for actual wind tunnel testing (C7*), and is representative of C7 that was analyzed in the anechoic chamber phase of testing. While not shown in these photographs, the portion of the south wall directly behind the linear array was treated with a vertical arrangement of the same material and dimensions as the acoustic wedges shown in Figure 7(a) for all of these configurations.

2.3. Data Processing Methods

Speaker waveform and microphone data were simultaneously acquired for both phases of testing. This allowed for the calculation of metrics such as propagation times, coherence, and transfer functions. Data were acquired in both testing phases for a total time duration of 60 seconds at a sampling rate of 65,536 samples per second using National Instruments PXIe 449x series dynamic signal acquisition cards installed in a PXIe 108x series chassis. Linear microphone array data in the wind tunnel were also simultaneously acquired at a higher sampling rate of 204,800 samples per second to diagnose higher frequency phenomena in the facility. Because all waveforms used in this study are BLWN random signals, all time-domain data are converted to the frequency domain using a Hanning window with 75% overlap between time blocks, using a narrowband frequency resolution of 16 Hz. All data are processed using the Signal Processing toolbox of MATLAB R2022a software.

Reflections are identified in this study using several processing metrics, including the autocorrelation and transfer functions between test setups. The autocorrelation is a measure of the similarity between the microphone time history and time-shifted (lagged) copies of the same time history. Reflections can be identified in an autocorrelation calculation by the occurrence of peaks at nonzero time delays in the autocorrelation. To determine the relative reflectivity effects of the different basket top configurations, a ratio of transfer functions is computed. A transfer function is computed as

$$H(f) = \frac{Y(f)}{X(f)}, \tag{1}$$

where $X(f)$ and $Y(f)$ represent the Fast Fourier Transform (FFT) of the system input and output, respectively. In this study, the system input is represented by the waveform supplied to the speaker, and the system outputs are the measurements made by the microphones. Figure 8 provides a process flow diagram of the transfer function ratio calculation procedure. As this figure shows, the ratio of transfer functions in this study is effectively a measure of the differences in measured acoustic spectra between a basket top configuration and the empty (fully treated) anechoic chamber.

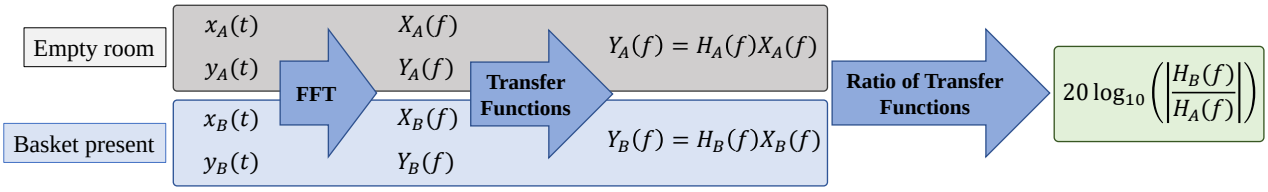

Figure 8: Flow chart illustrating signal processing steps for computing transfer function ratios between basket configuration runs. *Note that flow chart is representative of anechoic chamber measurements.*

An important underlying assumption of the transfer function calculation is that the system output is correlated with the system input. To ensure this condition is satisfied, cross-correlations are computed between the microphone signals and the supplied waveform signal, effectively providing the sound propagation time delay. The microphone signals are then time-shifted to align with the waveform signal, and the magnitude-squared coherence, $\gamma^2_{xy}(f)$, is calculated. Strong coherence between the waveform signal and microphones was verified for empty chamber conditions with $\gamma^2_{xy} > 0.8$ for the frequency ranges considered. It is important to note that the transfer function ratio calculations described here are done so in the context of the SALT anechoic chamber setup. Similar data processing is performed for the wind tunnel phase of experiments, however with a less optimal reference configuration that is discussed in Section 2.2.

3. RESULTS AND DISCUSSION

3.1. Single-Basket Reflectivity Assessment

Figure 9 provides the autocorrelations and autospectral densities of SALT microphones 1-3 (ordered top to bottom) for the cases of an empty chamber (C1) and an acoustic basket outfit with a plywood cover (C3). Note that in addition to the autocorrelations themselves in Figure 9(a),

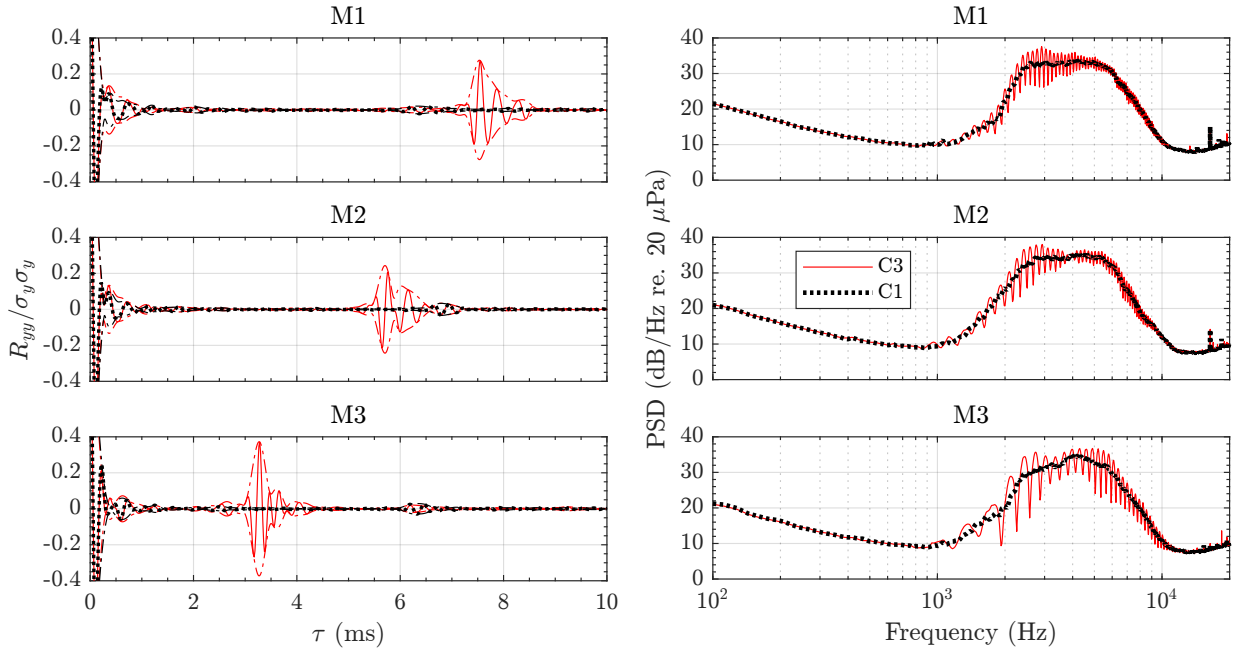

(a) Autocorrelations (b) Autospectral Densities

Figure 9: Examples of (a) autocorrelation and (b) autospectral density processing applied to SALT microphone data. *Note: data in this figure represent those for configurations C1 and C3 detailed in Figure 5 for the 4 kHz-centered octave band waveform signal. Analytical envelope functions of measured autocorrelations are represented by – · – lines in (a).*

an analytical envelope function computed via the Hilbert transform is also provided for each autocorrelation. This envelope function will be utilized later in this section as a visual aid for comparison between different basket top configurations. As is to be expected, prominent reflections are visible in this figure in the forms of both correlation peaks at nonzero time delays (τ) in Figure 9(a) and prominent spectral ripple in the autospectra of Figure 9(b) for configuration 3. The trend of decreasing time delay of the autocorrelation ripple from top (microphone 1) to bottom (microphone 3) represents the decrease in the difference between the path lengths of the reflected and direct waves.

Figure 10 provides the transfer function magnitude and ratio calculations for the SALT microphones for the cases of the empty treated chamber (C1) and the notionally acoustically hard plywood sheet basket top cover (C3). These test configurations represent conditions A and B in the flow chart of Figure 8, respectively. As can be seen in Figure 10(a), the transfer function magnitudes are defined in terms of the measured output of the microphones in units of Pascals (Pa) relative to the speaker waveform input into the system in volts (V). Furthermore, the spectral ripple associated with C3 is indicative of the strong reflections present in the data due to the presence of the plywood basket cover. The transfer function ratios for all three microphones are provided in Figure 10(b). These data are presented both as a function of dimensional frequency (f), as well as in terms of a nondimensional frequency coefficient, $f \cdot \Delta R / c_\infty$, where ΔR represents the difference in path lengths between the reflected and incident sound waves, and c_∞ represents the ambient speed of sound in the facility [8]. This frequency nondimensionalization allows for the viewing of the signal constructive and destructive interference patterns on a common basis

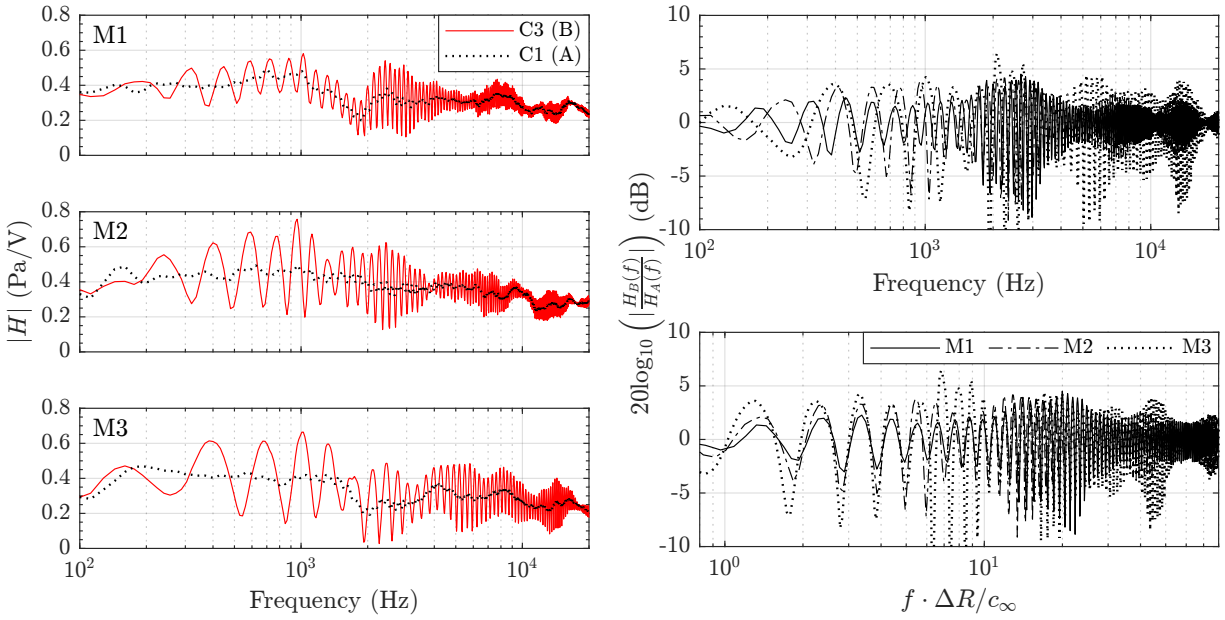

(a) Transfer Function Magnitudes

(b) Transfer Function Ratios

Figure 10: Transfer function (a) magnitude and (b) ratio calculations for notional acoustically hard basket top configuration (C3, plywood sheet). *Note: results represent those for the full spectrum BLWN signal; microphones 1 - 3 ordered top to bottom in (a).*

for different observation angles. The frequency scaling parameter $\Delta R/c_\infty = \tau_{\Delta R}$ is approximated through use of the analytic envelope function applied to the microphone autocorrelation for the case of a strong reflection (C3). This identification method was found to work very well using the case of the 8 kHz-centered BLWN waveform, where the peak amplitude of the autocorrelation envelope was approximated as $\tau_{\Delta R}$. It is worth noting that the overall amplitudes of spectral ripple are seen to intensify with increasing microphone number, which is believed to be due to the decrease in distance between the reflecting surface and the microphone.

Figure 11 provides the positive component of the autocorrelation envelope of microphone 2 for all tested configurations illustrated in Figure 5 for the case of an 8 kHz-centered octave band BLWN waveform signal. The results clearly show prominent reflected energy for configurations C3, C5, and C6, with C3 being the obvious worst-case. Furthermore, there is a nearly indiscernible difference between C1 and C2, which is a strong testament to the excellent absorptive behavior of the exposed variable-density basket foam. Meanwhile, C4 and C7 show slight indications of reflectivity, but require more detailed analysis.

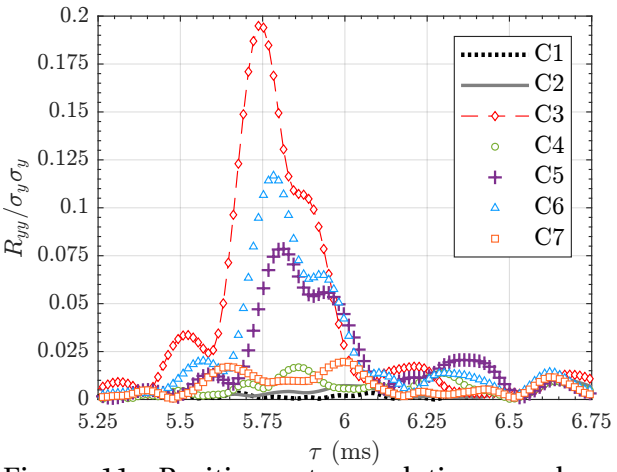

Figure 11: Positive autocorrelation envelope of microphone 2 for all basket configurations. *Note: 8 kHz octave band BLWN signal used.*

Figure 12 provides the transfer function ratios of microphone 2 for the six basket top configurations relative to the empty chamber configuration, with the most reflective being shown in Figure 12(a) and the least reflective being shown in Figure 12(b). These results clearly indicate that presence of perforate paneling causes prominent reflectivity for microphone measurements at an oblique angle relative to the panel. The presence of adhesive-backed felt on the perforate panel is seen to increase the reflectivity, which is not surprising due to the nonporous adhesive layer below the felt. Finally, the results of Figure 12(b) show that C7 performs slightly worse than C4, which is believed to be due to the

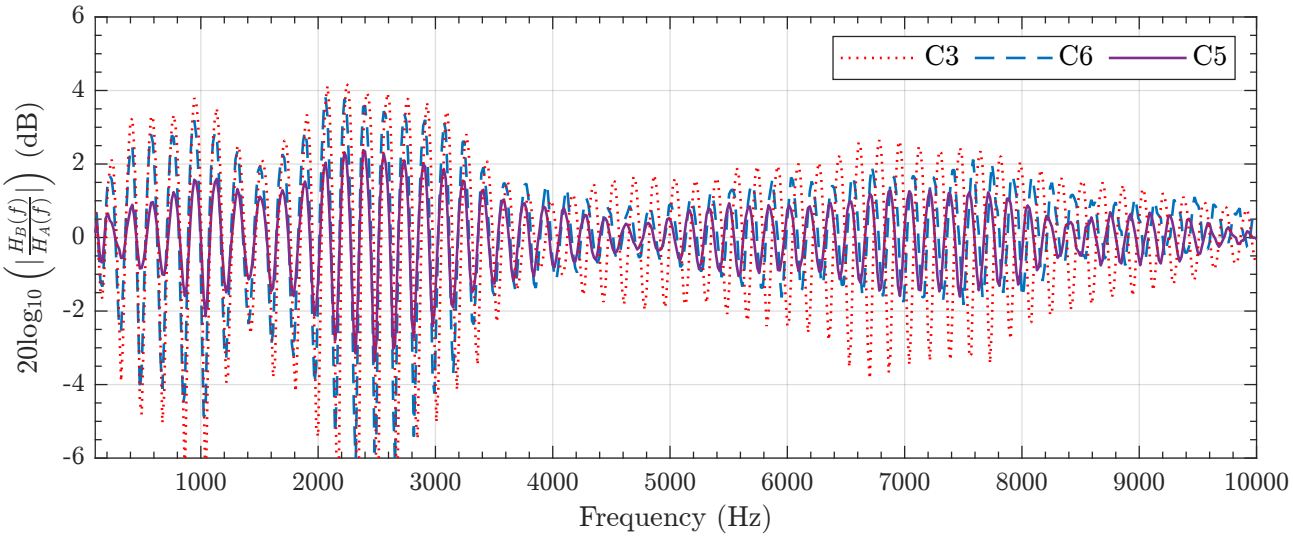

(a)

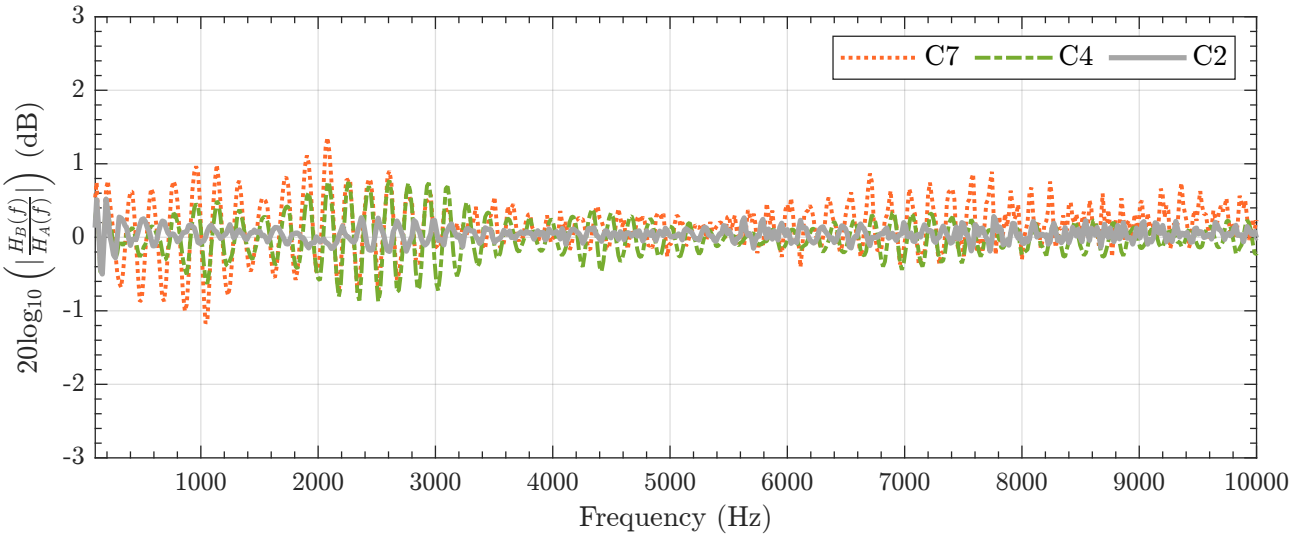

(b)

Figure 12: Transfer function ratios of microphone 2 for the (a) most-reflective and (b) least-reflective basket top configurations (defined in Figure 5) using the full-spectrum BLWN waveform signal. *Note: different dB limits for (a) and (b); shown only up to 10 kHz for visual clarity.*

presence of the compacted fibers of the felt over the basket top of C4. Levels of spectral ripple are found to remain approximately within ± 1.3 dB across the entire tested frequency range for C7, while those for C4 remain within ± 1 dB. This only slight increase in reflectivity coupled with the previously determined reduction in flow scrubbing noise over felt as compared to open-cell foam [3], makes C7 an excellent candidate for wind tunnel testing.

Figure 13 provides a component breakdown of configuration 7. This configuration is intended to capitalize on the benefits of the legacy configurations of Figure 3, while also reducing the detrimental aspects of them as well. The nonadhesive felt top layer of the basket is intended to reduce aerodynamic scrubbing noise as compared to the exposed open-cell foam sheet top layer of Figure 3(a), while also inducing less reflectivity associated with the perforate paneling and adhesive-backed felt top layers of Figure 3(b).

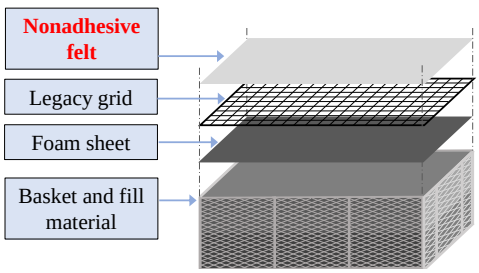

Figure 13: Component breakdown of newly designed acoustic basket (configuration 7).

3.2. Wind Tunnel Floor Reflectivity Assessment

The reflectivity of the floor treatment is assessed in the empty test section of the 14x22 with the use of the linear tower array discussed in Section 2.2. Specifically, microphone 8 will be the focus because it represents a nearly zero-degree angle of incidence relative to the speaker source, which is most comparable to microphone 2 of the SALT anechoic chamber test setup. Figure 14 provides the positive autocorrelation envelopes of the 14x22 test section floor installations. Note that the speaker waveform utilized in the 14x22 was a BLWN signal that spanned a frequency range of 100 Hz to 20 kHz. Therefore, in an effort to more directly compare the autocorrelation results between the two tests, a bandpass filter was applied to the autocorrelation data of Figure 14 that excluded frequencies outside of the 8 kHz-centered octave band. The positive autocorrelation envelopes in Figure 14 clearly show a prominent reflection for the case of plywood panel floor coverings (C3*), with only a slight difference between the cases of the completed basket tops (C7*) and basket tops covered with acoustic wedges (C1*). These results bear a strong resemblance to those presented in Figure 11 for the SALT measurement setup, however with different overall levels between the autocorrelations. The higher levels shown in Figure 14 are believed to be due to the shorter path length of the reflected waves relative to the direct path length as compared to those for the SALT chamber test setup. It is also possible, however, that differences in the speaker directivity of the direct and reflected waves between test setups are a contributing factor. The differences in reflection paths relative to their respective direct paths is evident by the earlier time of the autocorrelation peak for the plywood panel case in Figure 14 of $\tau_{\Delta R} \approx 2.9$ ms rather than the $\tau_{\Delta R} \approx 5.75$ ms shown in Figure 11.

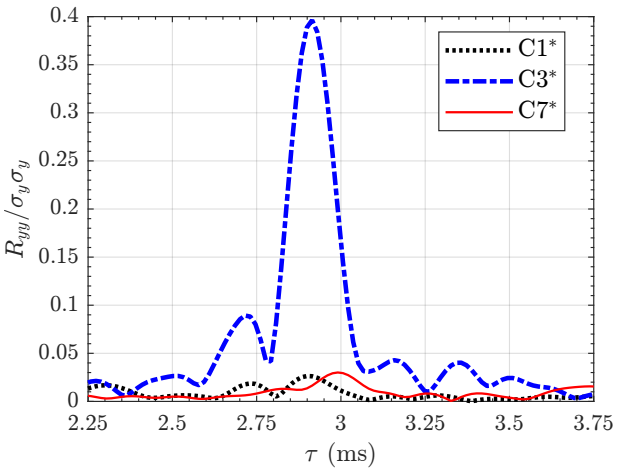

Figure 14: Positive autocorrelation envelope of microphone 8 for test section floor treatment conditions of Figure 7.

Figure 15 shows the transfer function ratios for the plywood panel basket coverings (C3*) and the newly designed basket configuration (C7*) relative to the reference condition (C1*). The

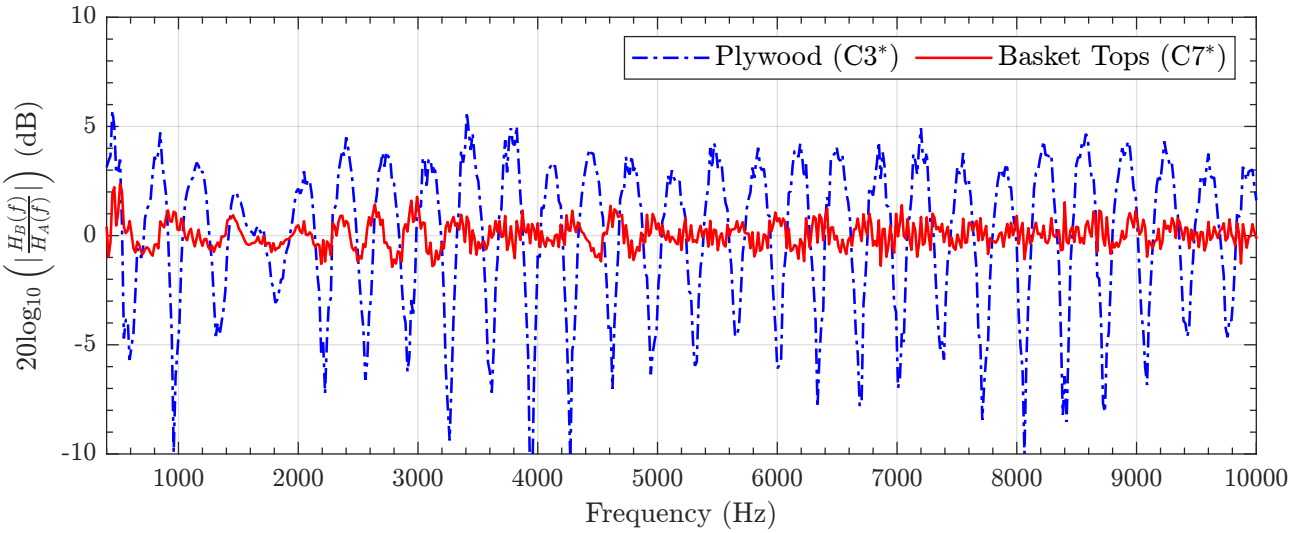

Figure 15: Transfer function ratios of linear array microphone 8 for the cases of plywood panel coverings (C3*) and completed floor basket (C7*) in the 14x22 test section. *Note: transfer function ratios are computed relative to the reference case of acoustic wedges placed on top of baskets (C1*); shown only up to 10 kHz for visual clarity.*

results show that the spectral variance of the newly designed acoustic baskets remains within ± 2 dB for frequencies above 400 Hz. Note that a frequency lower limit of 400 Hz was interrogated for this calculation because it represents the approximate cut-on absorption frequency of the acoustic wedges used in the in-situ reference condition (see Figure 7(a)). These results provide evidence both that the new basket top configuration detailed in Figure 13 offers good absorption characteristics and that the simplified and more controlled anechoic chamber measurements of the first phase of testing are a suitable diagnostic setup.

3.3. Wind Tunnel Facility Flow Noise Assessment

With the reflectivity of the 14x22 test section floor assessed using the new basket top design, the aerodynamic scrubbing noise of the new configuration will be assessed. This is done by a simple single-microphone comparison of common wind tunnel operating conditions (flow speeds) between the previous floor basket configuration (see Figures 1(b) and 3(b)) and the current configuration (see Figures 6(b) and 13) for an empty test section (i.e., no CRM-HL model is installed for the legacy measurement condition). It is important to note that this comparison is not intended to point directly at the test section floor treatment as the sole explanation for differences between the measurements, but rather to ensure that there are no appreciable differences in empty test section flow noise between configurations. Figure 16 provides narrowband acoustic spectra comparisons between the present and previous CRM-HL test entries for an empty test section at several flow speeds. A 6 dB subtraction is applied to the CRM-HL measurement data in an attempt to account for the pressure-doubling effect as a result of the flush-mounted microphone installation in the phased array for that test. Furthermore, the CRM-HL measurement data are compared to data of linear array microphone 7 of the current test (see Figure 6(a)) because this microphone represents the measurement location of closest proximity to the CRM-HL microphone. The spectra show very good agreement, with the present test data exhibiting only slightly higher noise levels across an approximate frequency range of $3 \leq f \leq 12$ kHz for the speeds shown. Figure 17 provides a comparison of the integrated overall sound pressure levels (OASPLs) for a range of flow speeds between the two test entries, computed over a common frequency range of $100 \leq f \leq 60{,}000$ Hz.

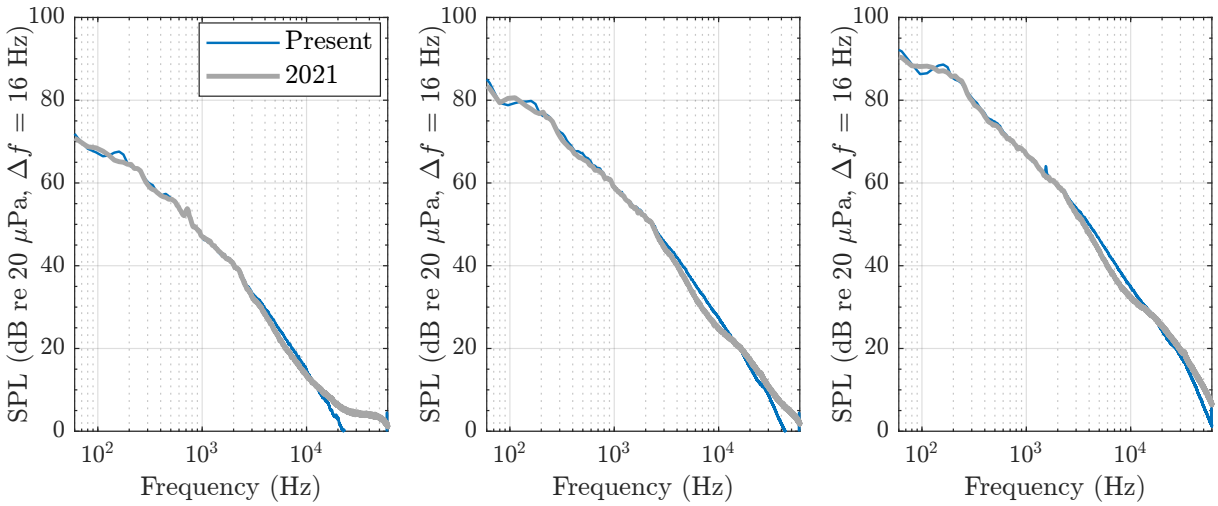

(a) $M_\infty = 0.08$ (b) $M_\infty = 0.12$ (c) $M_\infty = 0.16$

Figure 16: Empty test section narrowband acoustic spectra comparisons between present 14x22 tunnel entry and previous entry for tunnel speeds of (a) $M_\infty = 0.08$, (b) $M_\infty = 0.12$, and (c) $M_\infty = 0.16$. *Note: linear tower array microphone 7 in the present study compared with phased array center microphone for the CRM-HL 2021 entry (see Figure 1(b)); no test models are present in the test section for either data set.*

These results convey a trend similar to that shown in Figure 16, where the present entry displays marginally higher overall levels over the majority of tested flow speeds. The facility run condition for which the current data set OASPLs most exceed those of the CRM-HL data set is at M_∞ = 0.20, the difference of which is approximately 1 dB. It is worth noting that these two test entries occurred at different times of the year, resulting in very different ambient conditions within the test cell. There were average temperature differences of approximately 10^o Celsius and average relative humidity differences of 15% between these data sets, with the present test being on the high end. As a result of these differences in ambient conditions, it is difficult to relate the acoustic measurements to each other because of unique hydrodynamic noise behaviors generated by flow through the wind tunnel open test section as well as the noise generated by the wind tunnel fan itself. Furthermore, the 14x22 tunnel circuit is equipped with a flap ventilation system that can be used to decrease temperatures in the facility. Opening of these flaps in the present entry was found to result in increased low frequency facility noise levels, yielding between 1 and 3 dB increases in the OASPLs of Figure 17 depending on flow speed. Despite these complicating factors, the SPL spectra and OASPL comparisons are believed to be sufficient in demonstrating that the modifications to the acoustic baskets in the present test have not appreciably added to the facility background noise measured in the previous entry.

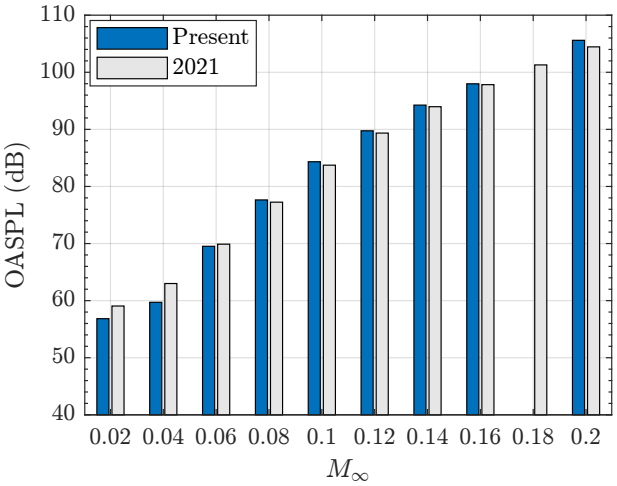

Figure 17: Empty test section OASPL comparisons between present and 2021 entries in the 14x22 over a range of flow speeds.

4. SUMMARY AND CONCLUSIONS

A two-phase test campaign was implemented to identify the suitability of an updated floor basket treatment configuration for acoustic testing in the NASA Langley 14- by 22-Foot Subsonic Tunnel. The two phases were comprised of microphone measurements in an anechoic chamber to assess the reflectivity of a single basket of various top treatments at oblique angles of incidence, as well as in-situ assessments of basket top reflectivity and aerodynamic flow scrubbing noise in the wind tunnel itself. It was found that a previous acoustic basket top configuration implemented in a 2021 test entry suffers from prominent reflectivity due to the combined presence of a perforate metal panel and a layer of felt with adhesive backing. This configuration was previously implemented because the high frequency range of interest associated with the scaled CRM-HL airframe noise model resulted in a prominent focus on aerodynamic scrubbing noise mitigation, with less concern on floor reflections. The use of adhesive-backed felt as a top layer provided enough absorption at high frequencies and a considerable reduction in aerodynamic scrubbing noise relative to previous implementations to make it a suitable candidate. The latest implementation capitalizes on the benefit offered by the 2021 configuration of reduced scrubbing noise associated with flow over felt, but without the acoustically hard felt adhesive backing and perforate paneling. Utilizing a nonadhesive felt covering over a large-percentage open area metal grid that is used to secure acoustic foam basket fill material yielded only marginal increases in reflectivity relative to this same configuration without the felt. In-situ reflectivity measurements in the wind tunnel corroborated the findings of the anechoic chamber test, and empty test section flow noise measurements confirmed excellent similarities to noise measurements made in the 2021 entry. Thus, the newly designed acoustic basket tops are believed to be a suitable alternative to the previous iterations by performing well both in terms of acoustic absorptivity over a wide frequency range, and reduced aerodynamic scrubbing noise relative to flow over open-cell foam.

ACKNOWLEDGMENTS

The authors would like to acknowledge Stephanie Heath of the NASA Langley Aeroacoustics Branch for her modeling efforts of acoustic basket media and for her invaluable guidance. The authors would also like to acknowledge Florence Hutcheson and Christopher Bahr of the Aeroacoustics Branch, Tony Humphreys of the Research Directorate, and David Lockard of the Computational AeroSciences Branch for their historical data provision and insights. Jaye Moen of the Aeroacoustics Branch is also gratefully acknowledged for his assistance with anechoic chamber test setup. Finally, the authors would like to acknowledge the NASA Langley 14- by 22-Foot Subsonic Tunnel and Low Speed Aeroacoustic Wind Tunnel staff for their tireless efforts in making the acoustics facility characterization effort a success. This work was funded by the NASA Revolutionary Vertical Lift Technology (RVLT) project.

REFERENCES

1. M. A. Marcolini, D. A. Conner, J. T. Brieger, L. E. Becker, and C. D. Smith. Noise Characteristics of a Model Tiltrotor. In *AHS 51st Annual Forum and Technology Display*, Fort Worth, TX, May 1995.
2. D. P. Lockard, T. L. Turner, C. J. Bahr, and F. V. Hutcheson. Overview of Aeroacoustic Testing of the High-Lift Common Research Model. In *AIAA AVIATION 2021 Forum*, AIAA Paper 2021-2113, Virtual Event, August 2021.
3. F. V. Hutcheson, D. P. Lockard, and D. Stead. On the Alleviation of Background Noise for the High-Lift Common Research Model Aeroacoustic Test. In *28th AIAA/CEAS Aeroacoustics 2022 Conference*, AIAA Paper 2022-2988, Southampton, UK, June 2022.
4. F. W. Grosveld. Calibration of the Structural Acoustics Loads and Transmission Facility at NASA Langley Research Center. In *InterNoise 99*, Fort Lauderdale, FL, December 1999.
5. C. M. Stutz, M. L. Houston, N. S. Zawodny, and K. A. Pascioni. Acoustic Characterization of the NASA Langley 14- by 22-Foot Subsonic Tunnel Using Single-Microphone Analysis Techniques. In *Proceeding of Noise-Con 2024*, New Orleans, LA, June 2024.
6. M. L. Houston, C. M. Stutz, N. S. Zawodny, and K. A. Pascioni. Acoustic Characterization of the NASA Langley 14- by 22-Foot Subsonic Tunnel using a Phased Array. In *Proceeding of Noise-Con 2024*, New Orleans, LA, June 2024.
7. W. C. Horne and N. Burnside. Initial Calibrations and Wind Tunnel Test Results for an In-Flow Reference Array Using New In-Flow Acoustic Sources in Four Array Mount Configurations. In *2018 AIAA/CEAS Aeroacoustics Conference*, AIAA Paper 2018-2969, Atlanta, GA, June 2018.
8. B. N. Shivashankara and G. W. Stubbs. Ground plane microphone for measurement of aircraft flyover noise. *Journal of Aircraft*, 24(11):751–758, 1987.